How to efficiently intercalate alkaline-earth metals into graphite using LiCl-KCl molten salts

Inass El Hajj, Lucie Speyer, Sébastien Cahen, Pascal Berger, Ghouti Medjahdi, Philippe Lagrange, Claire Hérold

How to efficiently intercalate alkaline-earth metals into graphite using LiCl-KCl molten salts: an overview on the case of barium

Inass El Hajj[a], Lucie Speyer[a], Sébastien Cahen[a], Pascal Berger[b], Ghouti Medjahdi[a], Philippe Lagrange[a], Claire Hérold[a 1]

[a] IJL, Université de Lorraine, CNRS, 2 allée André Guinier, 54011 Nancy cedex, France

[b] NIMBE, CEA, CNRS, Université Paris-Saclay, CEA Saclay, 91191 Gif sur Yvette cedex, France

Abstract

In this paper, we present the three first stages currently known Ba-based Graphite Intercalation Compounds (GIC). They are synthesized using the LiCl-KCl molten salts method, which is especially efficient in order to help the intercalation of barium into the 2D graphitic galleries. According to the chosen reaction conditions, it is possible to obtain either the BaC_6 binary compound or one of the two quaternary phases whose intercalated sheets contain simultaneously lithium, potassium and barium. By combining X-ray diffraction measurements and ion beam analyses for these compounds, their chemical formula is well established: $Li_{0.2}K_{0.6}Ba_{0.35}C_6$ for the α-phase, $Li_{0.2}K_{0.75}Ba_{0.6}C_6$ for the β one and BaC_6 for the binary.

The intercalated sheets of this last compound are single-layered. Its repeat distance reaches 529 pm and its 2D unit cell is hexagonal and commensurate with the graphene one with a parameter of 430.6 pm. However, α- and β-phases are much more complex. For α compound, the intercalated sheets are three-layered with an interplanar distance of 650 pm, while for β-phase, they are six-layered and the interplanar distance reaches 950 pm. Both 2D unit cells are hexagonal, with a planar lattice parameter a of 1074 pm and 1280 pm respectively.

Finally, a model of reaction mechanism is proposed, which breaks down the intercalation process into several steps: intercalation of lithium (LiC_6), then replacement by barium (BaC_6), next,

[1] claire.herold@univ-lorraine.fr
Institut Jean Lamour - UMR 7198 CNRS-Université de Lorraine
Campus ARTEM - 2 Allée André Guinier
B.P. 50840 F54011 Nancy Cedex

formation of the β-phase, and ultimately its elimination to the benefit of the α one. Thus, this latter appears as the most stable GIC in this LiCl-KCl molten medium.

Keywords

Graphite intercalation compounds, barium, molten salts, X-ray diffraction, mechanism

Introduction

Due to its amphoteric character, graphite, which is a stacking of graphene planes, is able to host electron donor or electron acceptor chemical species in its Van der Waals's two-dimensional galleries. Especially, the strongly electropositive metals intercalate very easily into graphite [1]. Thus, at low temperatures, the vapors of potassium, rubidium and cesium react with graphite leading to first stage lamellar Graphite Intercalation Compounds (GIC) of MC_8 formula (M = K, Rb and Cs) by a solid-vapor reaction. Even if such a reaction is more difficult in the case of lithium, it is however possible to obtain with this alkali metal a first stage GIC much richer in metal than the previous ones since its formula is indeed LiC_6.

This binary GIC has been discovered in our team in 1955 [2] and completely characterized in 1975 [3]. It is immensely known today and used around the world in the technology of the Li-ion batteries [4], since it constitutes the negative electrode of these devices, whose applications are at this time particularly numerous. Huge efforts are currently performed in order to replace lithium with another metal. In this particular context, we have conducted an academic widened study concerning the intercalation of alkaline-earth metals into graphite, calcium, strontium and barium [5,6], which are also highly electropositive metals and form divalent ions interesting for battery applications.

Elsewhere, it is demonstrated that the binary alkaline-earth metals GIC become superconducting at low temperature [7-9] with an evolution of the critical temperature depending on the nature of the intercalated element and the structure of the GIC. This noteworthy physical property also greatly motivates the interest of this study.

Considering the direct intercalation of such elements, the vapor pressure of the alkaline-earth metals is much weaker than that of the alkali metals. Therefore, the use of the solid-vapor

method requires an increase of the reaction temperature in order to raise the vapor pressure. Even in these conditions, the intercalation reaction occurs only very weakly and the formation of the GIC remains strictly superficial [10]. Moreover, if the reaction temperature is increased, the graphene planes are destroyed and metallic carbides are formed, resulting from this drastic damage. In the end, the solid-vapor method remains poorly efficient as intercalation strategy for these elements. Fortunately, there are other routes developed in our team able to synthesize bulk binary first-stage MC_6 (M = Ca, Sr and Ba) compounds.

A very helpful method implements a chemical reaction between a bulk graphite sample and a liquid metallic alloy by solid-liquid process. It has been demonstrated that calcium or barium can be fully intercalated into the bulk of graphite to form CaC_6 or BaC_6 using corresponding binary lithium alloys [5]. Surprisingly, it has been possible to synthesize several two-dimensional ternary compounds containing both lithium and calcium [11].

Another very efficient solid-liquid method consists in performing a reaction between graphite and a solution of the alkaline-earth metal in the LiCl-KCl molten eutectic [12]. As previously, by this means, the intercalation of the dissolved metal occurs and has enabled for instance to synthesize the first stage BaC_6 graphite-barium compound showing the highest quality observed until now [13]. Furthermore, this method makes it possible to synthesize lamellar quaternary phases including simultaneously lithium, potassium and the alkaline-earth element [14,15].

In this paper, we are aspiring to describe all the first stage Ba-based known GIC prepared by the aforementioned molten salts method: optimal synthesis conditions and crystal structure. These compounds are in the number of three, the formerly reported binary phase and two quaternary ones, which are novel lamellar materials recently discovered in our group.

Experimental

Synthesis

All experiments are carried out in a glove box under purified argon atmosphere in order to avoid the degradation of the highly air- and moisture-sensitive materials used for the syntheses and the prepared GIC. Lithium and potassium chlorides (purity 99%) are previously degassed overnight

at 240°C under secondary vacuum, then mixed in the glove box by following the eutectic composition (58.2 mol% LiCl and 41.8 mol% KCl [16]). 4 g of the eutectic mixture are introduced in a stainless-steel reactor and melted by heating at 450°C. Then, 2 at.% of barium are introduced (about 200 mg, purity 99.9 %), so that it is in excess versus graphite and then its chemical activity is not modified during the reaction. The blend is manually stirred until barium is completely dissolved and a platelet of pyrolytic graphite (25 mg) is plunged inside the reactor, which is tightly closed and transferred in a metal enclosure to be heated outside the glovebox. The heating is carried out at 450°C during several days, then the reactor is reintroduced in the glovebox. The reactor is re-heated in order to melt the reaction medium and extract the sample, which is manually scrapped to remove the salts at its surface, and stored in a glass capillary for X-ray characterization.

The optimal synthesis parameters were determined for each of the aforementioned three phases. BaC_6 is synthesized, as reported before, by stirring the reaction medium during 15 minutes inside the glovebox, then by conducting the heating during 12 days and by regularly swaying the furnace [13]. For the novel quaternary phases, only a quick stirring of the reaction medium is necessary before introducing graphite. Then, the synthesis reactor undergoes regular swaying during heating after a few days of reaction. After 12 days, an indigo compound, further denoted β-phase, is obtained [15]. For more than 12 days, a light blue compound, further denoted α-phase, is evidenced. The key parameters which are driving the intercalation reactions towards these different phases seem to be the dissolution of barium in the eutectic mixture, and the heating duration.

X-ray characterization

X-ray measurements are carried out with a Bruker D8 Advance diffractometer ($\lambda_{MoK\alpha1}$ = 70.926 pm) with a θ-2θ configuration and a 2.5° Soller slit. As samples are prepared from pyrolytic graphite, their crystallites are randomly oriented along (ab) planes but parallel along c-axis, so that they behave like a powder in the (ab) plane and like a single crystal along c-axis: the 00*l* and *hk*0 reflections can be separately recorded by modifying the sample orientation against the X-ray beam. The stacking sequences along c-axis are determined from the quantitative analysis of the 00*l* reflections [17].

Rotating crystal patterns are acquired with a Bruker Kappa APEX Duo diffractometer having a two-dimensional CCD APEX II detector and a X-ray micro-source with a 100 mm diameter spot. A small piece (some hundreds of microns) of the sample is cut, then introduced in a Lindemann glass capillary (0.5 mm diameter) and placed in the diffractometer with its c-axis normal to the incident beam. Thanks to the polycrystalline character of the graphene planes, as previously mentioned, it is easy to record very distinctly and without any rotation the 00*l*, *hk*0 and *hkl* reflections.

Ion beam analysis

Ion beam analysis allows the study of the chemical composition, including light elements, with lateral and in-depth resolution capabilities to look for the homogeneity of a sample. Samples were investigated with a 3 MeV proton beam (3 x 3 μm^2), and analyzed with a particle detector at 170° from the incident beam axis. Elements are mapped on 200 x 200 μm^2 areas. For the heaviest elements, only the backscattering between the proton ion beam and the target occurs. For Ba, Rutherford backscattering on $^{134\text{-}138}$Ba isotopes (mainly ^{137}Ba(p, p)^{137}Ba) of surface protons are scattered at 2900 keV. For C, O, Cl and K, cross-sections (probability of scattering) differ from Rutherford law. References of the non-Rutherford cross-sections sets used for spectra simulation are listed below:

- Backscattering on carbon ^{12}C(p, p)^{12}C, [18], backscattered protons are emitted at 2145 keV;

- Backscattering on oxygen ^{16}O(p, p)^{16}O, [19], backscattered protons are emitted at 2320 keV;

- Backscattering on chlorine ^{nat}Cl(p, p)^{nat}Cl, [20], backscattered protons are emitted at 2670 keV;

- Backscattering on potassium ^{nat}K(p, p)^{nat}K, [21], backscattered protons are emitted at 2700 keV;

In the case of lithium, both backscattering and nuclear reaction must be taken in consideration. The corresponding interactions and their related energies are as follows:

- Nuclear reaction on ^{7}Li ^{7}Li(p, α)^{4}He (laboratory data). Surface α particles are emitted at 7450 keV;
- Backscattering on lithium ^{7}Li [22]; ^{7}Li(p, p)^{7}Li. Protons are backscattered from surface at 1680 keV;

- Backscattering on lithium ^{6}Li [22]; ^{6}Li(p, p)^{6}Li. Protons are backscattered from surface at 1530 keV.

The spectra are simulated with the SimNRA software for adjustment between experimental data and modeling [23]. A theoretical spectrum is calculated by modelling the sample by a stack of layers with adjustable chemical composition and thickness, which are optimized until the best accordance between theoretical and experimental spectra is obtained.

Results and discussion

1. Nominal composition from ion beam analysis

Representative RBS/NRA spectra of the different phases obtained in the Ba/LiCl-KCl system are given in Figure 1.

In such a spectrum, an element with homogeneous bulk concentration produces a flat step whereas a surface overconcentration produces a more or less sharp peak.

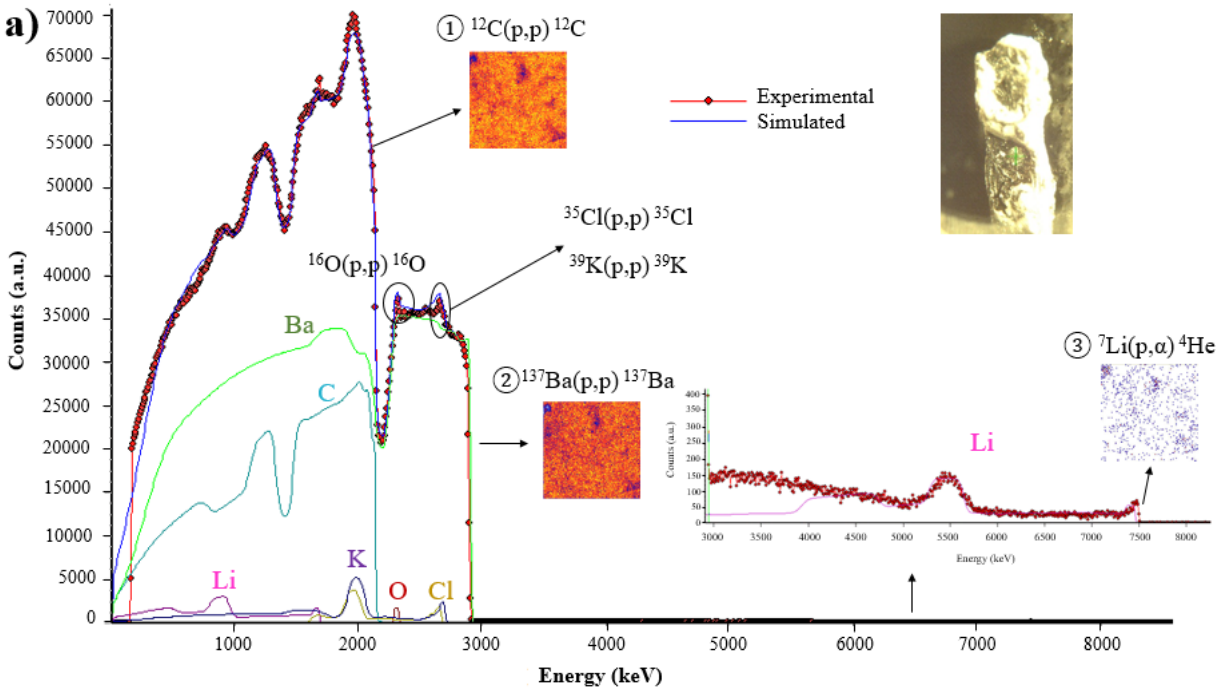
a)
Counts (a.u.)
Energy (keV)
① ^{12}C(p,p) ^{12}C
Experimental
Simulated
^{35}Cl(p,p) ^{35}Cl
^{39}K(p,p) ^{39}K
^{16}O(p,p) ^{16}O
Ba
C
② ^{137}Ba(p,p) ^{137}Ba
③ ^{7}Li(p,α) ^{4}He
Li
K
O
Cl

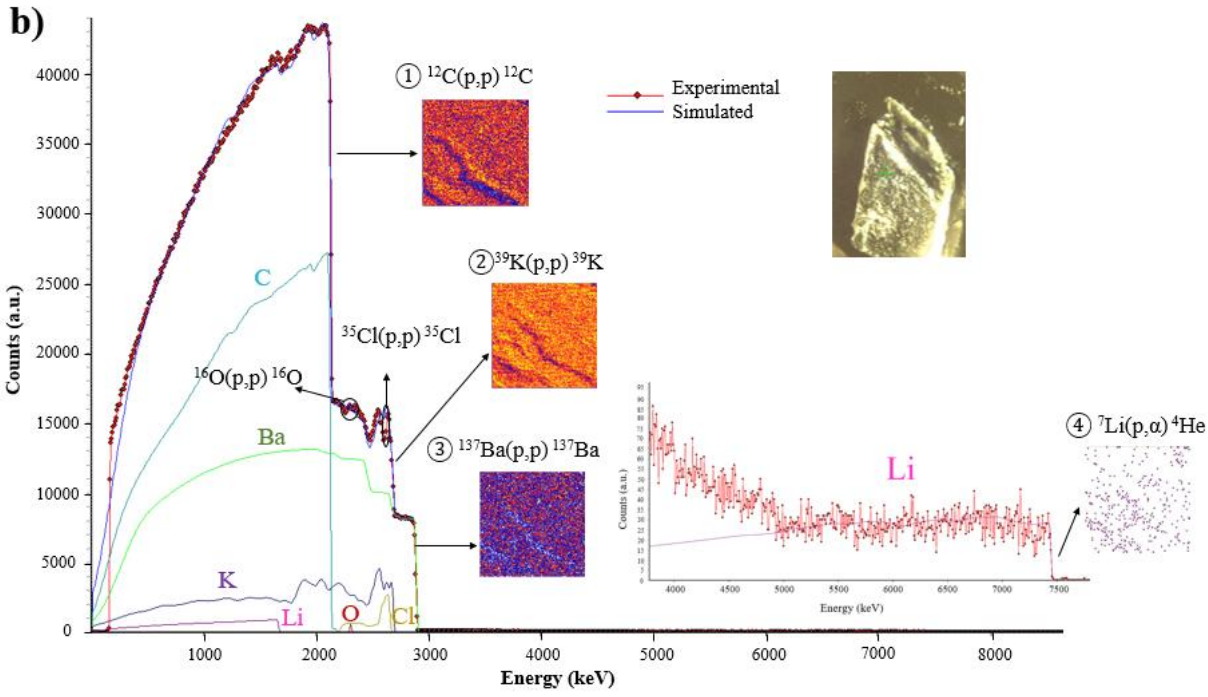
b)
Counts (a.u.)
Energy (keV)
① ^{12}C(p,p) ^{12}C
Experimental
Simulated
② ^{39}K(p,p) ^{39}K
C
^{35}Cl(p,p) ^{35}Cl
^{16}O(p,p) ^{16}O
Ba
③ ^{137}Ba(p,p) ^{137}Ba
④ ^{7}Li(p,α) ^{4}He
Li
K
Li
O
Cl

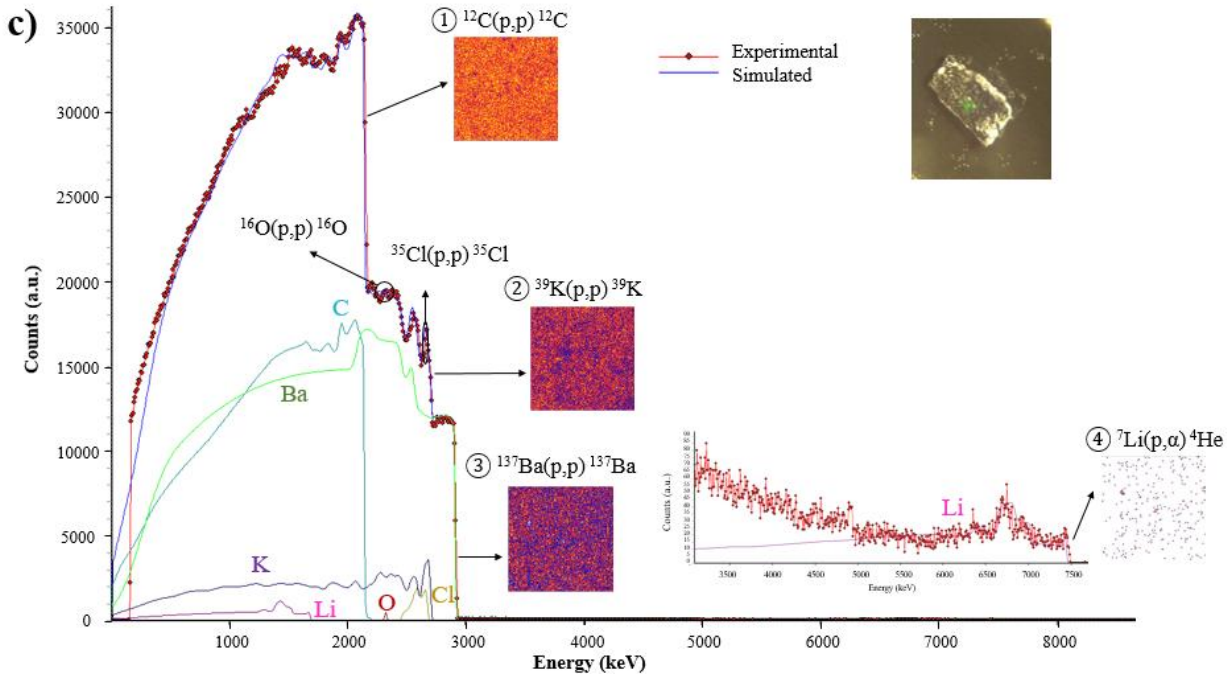

Fig. 1. Recorded RBS/NRA spectra of a) BaC_6 b) α-phase and c) β-phase and their simulation (with the contribution of each element). Inset shows a sample picture on the sample-holder of the microprobe instrument.

Figure 1a mainly reveals the presence of two steps around 2145 and 2900 keV, corresponding to C and Ba respectively. The adjustment of the experimental data agrees with the expected BaC_6 formula for the binary GIC. Moreover, the observation of the elementary mapping for these elements reveals a quite nice homogeneous distribution of carbon and barium laterally. One should note that residual lithium overconcentration into the bulk is detected at higher energy (2-3 atomic percent) and very small peaks in the 2300-2700 keV region due to residual impurities on the surface. Nevertheless, this result is in agreement with the obtention of a BaC_6 GIC intercalated into the bulk.

The RBS/NRA spectra of α and β phases are given Figure 1b and 1c. Both spectra show several steps at characteristic energies, what means the intercalation into the bulk of the corresponding C, K, and Ba elements. Moreover, associated elementary maps reveal that these elements are homogeneously distributed in the α-phase and β-phase. Very small peaks of residual O and Cl are also detected, due to impurities of the surface. The presence of oxygen is exclusively due to the rapid transfer in ambient atmosphere during the introduction of the samples in the analysis

chamber of the nuclear microprobe (surface slightly oxidized). Moreover, the weak chloride signal is due to a very small amount of tiny residual salts on the surface of the samples, after their scrapping. At higher energy corresponding to the $^{7}Li(p, \alpha)^{4}He$ nuclear reaction, lithium is also detected into the bulk. Even if some lithium veins can be detected (for instance a peak at 6700 keV for the β-phase Figure 1c), the signal due to nuclear reaction between the proton ion beam and lithium is almost constant, in agreement with an homogeneous in-depth repartition. Regarding the combination of the ion beam analysis (spectra and elementary maps) and 00*l* X-ray patterns and quantitative analyses in agreement with monophasic samples (see below), it must be concluded that this element is also intercalated together with potassium and barium between graphene layers. So, it is possible to adjust the experimental data with $Li_{0.2}K_{0.6}Ba_{0.35}C_6$ and $Li_{0.2}K_{0.75}Ba_{0.6}C_6$ nominal compositions for α-phase and β-phase respectively.

2. Structural studies

1D structure

The 00*l* X-ray diffraction patterns of the BaC_6 binary compound as well as those of the quaternary α and β phases are presented Fig. 2. In these three patterns, intense and individualized Bragg peaks correspond to the three bulk graphite intercalation compounds previously described. No more pristine graphite is observed. Very weak peaks are indexed as residual LiCl or KCl salts due to the reaction medium. Nevertheless, the color of the samples clearly appears and is very different for each compound. As other binary compounds containing an alkaline earth metal (SrC_6 and CaC_6), BaC_6 reveals a shiny silver color, whereas α and β phases present a light blue and indigo blue colors respectively.

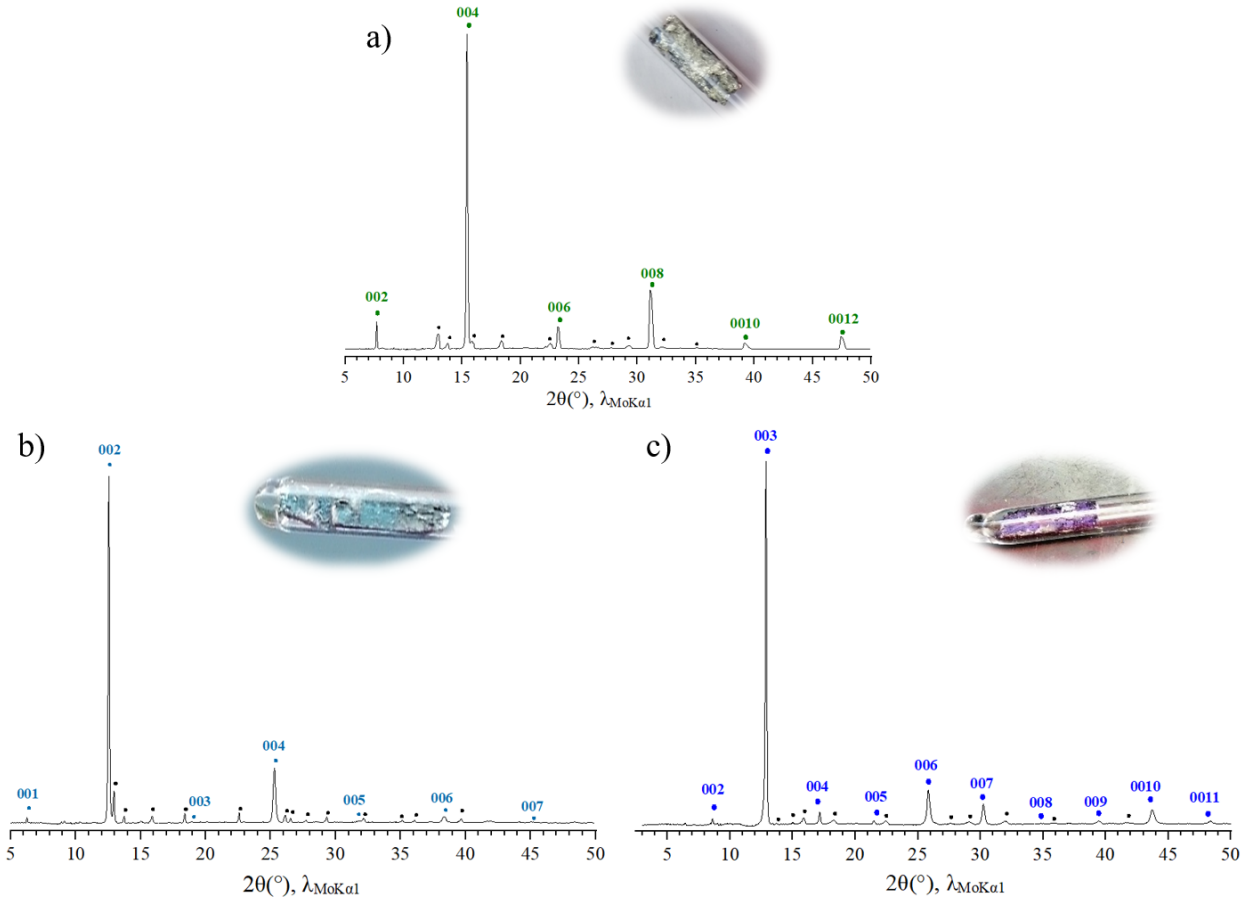

Fig. 2. 00*l* X-ray diffraction patterns and pictures of the corresponding samples of a) BaC_6, b) α-phase, c) β-phase

(●) LiCl or KCl ($ICDD_{LiCl}$: 04 016 2980 – $ICDD_{KCl}$: 04 007 3113)

The thicknesses of the recovered samples are very different too. Indeed, if the expansion of the samples along the c-axis is always clearly visible, α and β phases show an expansion much higher than that of the BaC_6 sample. These observed dilations are in favour of first stage compounds, and for each of the three patterns, the 00*l* reflections can be indexed considering a first stage compound. These reflections lead to the identification of the repeat distance, which are 529 pm, 650 pm and 950 pm for BaC_6, α-phase and β-phase respectively (Table 1). The quantitative study of the 00*l* reflections allows to determine the **c**-axis electronic density profiles. The 00*l* structure factors, calculated from a model taking into account the chemical formula deduced from ion beam analyses, are compared with those inferred from the diffracted intensities. For each phase, the corresponding **c**-axis electronic density profiles obtained by the

Fourier transform of experimental and calculated structure factors are then superimposed and the residual factor between both profiles is evaluated. Further details about this method can be retrieved in [17].

Table 1: Color and structural characteristics of the three Ba-based compounds

Compound	BaC_6	α-phase $Li_{0.2}K_{0.6}Ba_{0.35}C_6$	β-phase $Li_{0.2}K_{0.75}Ba_{0.6}C_6$
Color	shiny silver	light blue	Indigo blue
Repeat distance (pm)	529 ± 0.2	650 ± 1	950 ± 1
Intercalated sheets	single-layered	three-layered	six-layered

The electronic density profiles of the three compounds are shown Fig. 3; they indicate the best fit between the calculated and experimental profiles, thus to the lowest value of the residual factor. The corresponding schematic stacking sequences along the **c**-axis based on the chemical formula determined thanks to ion beam analyses are presented Fig. 4.

The best agreement between model and experience is obtained with a single-layered intercalated sheet for the binary BaC_6 compound, as previously reported [13]. In the case of the α-phase, as in BaC_6, the electronic density profile reveals a central plane of barium; the latter is however surrounded by two symmetrical layers containing lithium and potassium, leading to a three-layered intercalated sheet with a repeat distance I_c as expected slightly higher than that of BaC_6. The residual factor reaches 9.8%, without any thermal agitation correction factor. For the β-phase, the high repeat distance is explained by the stacking sequence which is K-Ba-(K/Li)-(Li/K)-Ba-K, corresponding to a six-layered intercalated sheet. Like for the α-phase, mixed lithium and potassium planes are present. The residual factor obtained for this model is 13.9% with a correction of Debye-Waller thermal factor of 0.3 $Å^2$. In both quaternary compounds, the potassium planes are close to the graphene sheets, ensuring an electronic transfer towards the latter. Moreover, these α and β compounds are very rich in metals (M = Li, K, Ba) since their general chemical formula could be written $M_{1.15}C_6$ and $M_{1.55}C_6$ respectively. The iono-metallic bonding in the intercalated sheets allows the coexistence of several metals in the interlayer space.

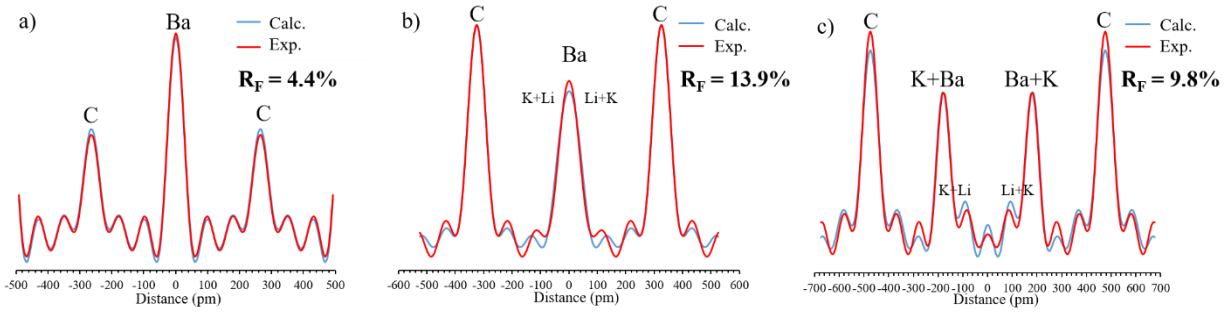

Fig. 3. Experimental and calculated 1D c-axis electronic density profiles of a) BaC_6, b) α-phase and c) β-phase

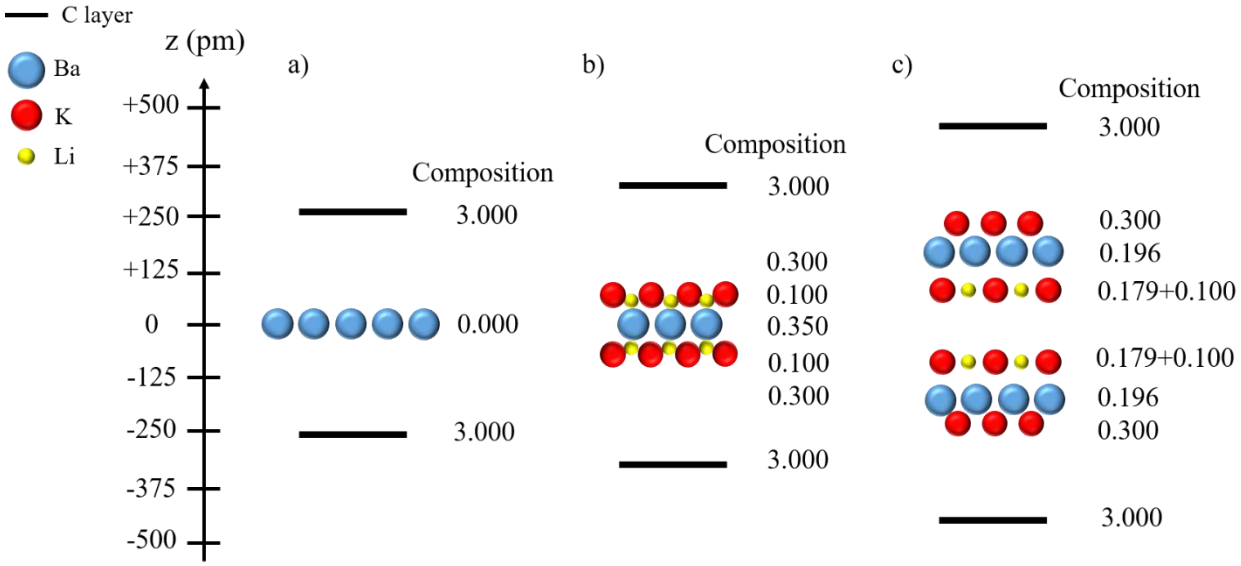

Fig. 4. Schematic stacking sequence along the **c**-axis of a) BaC_6, b) α-phase and c) β-phase

2D and 3D structures

The investigation of the structure of the three Ba-based compounds is continued by the study of the *hk*0 and *hkl* reflections. First, *hk*0 diffraction patterns were recorded for all samples (Fig. 5). In each diagram, a main family of reflections can be attributed to *hk*0 ones, accompanied by some weak reflections related to LiCl or KCl, or barium in the case of α-phase.

For BaC_6, all reflections can be indexed in the well-known two-dimensional hexal unit cell, which is commensurate with that of graphene planes. Indeed, for example, d_{110} and d_{300} of BaC_6

are respectively equivalent to d_{100} and d_{110} of graphite. The a parameter, calculated from the *hk*0 pattern, is equal to 430.6 pm, close to $a_g\sqrt{3}$ (a_g corresponds to the a parameter of graphite) and the 2D unit cell is rotated by 30° compared to that of graphite, leading to express the lattice by $(\sqrt{3}\times\sqrt{3})$ R30° (Fig. 6a).

In the case of the α-phase, the presence in the corresponding *hk*0 pattern (Fig. 5b) of three reflections at the theoretical positions of the 100, 110 and 200 reflections of graphite, clearly indicates that the intercalated network is commensurate with the graphitic one, since no pristine graphite is observed in the 00*l* diagram. Thanks to the model developed by Lagrange *et al.*, which gives the exhaustive 2D lattices commensurate with that of graphite for a given number of carbon atoms in a unit cell, it was possible to determine the only 2D unit cell leading to the observed *hk*0 reflections [24]. It is hexagonal with $a = a_g\sqrt{19} = 1074$ pm and contains 38 carbon atoms. It is rotated by 36° with respect to the graphene unit cell, which leads to its $(\sqrt{19} \times \sqrt{19})$ R36° expression (Fig. 6b).

The same mathematical approach was used to determine the 2D unit cell of the β-phase, since in this case also, despite the absence of graphite reflections in the 00*l* diagram indicating complete intercalation, three reflections are observed at the position of the *hk*0 graphite ones (Fig. 5c), allowing the conclusion of commensurability between the intercalated and graphene networks. Thus, using the previous mentioned model, the 2D unit cell was determined: although of hexagonal symmetry too, its parameters are higher than those of the α-phase, with $a = 3\, a_g\sqrt{3} = 1280$ pm, and the number of carbon atoms which reaches 54 is largely higher too. Moreover, the rotation with respect to the graphene lattice is of the classical value of 30°, leading to the 2D unit cell expression $(3\sqrt{3} \times 3\sqrt{3})$ R30° (Fig. 6c).

These 2D unit cells determined for both quaternary compounds are also very different from that of BaC_6.

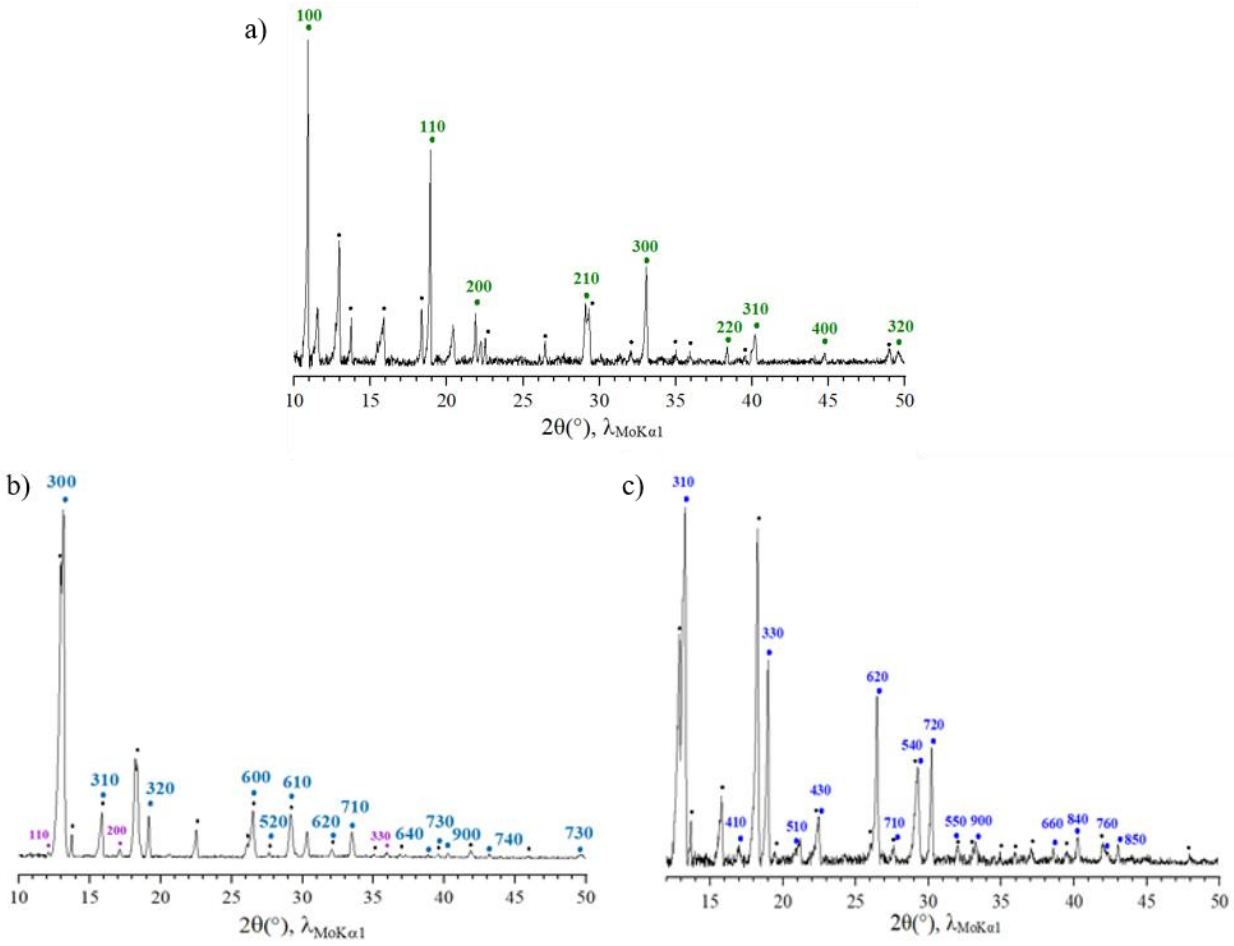

Fig. 5. *hk*0 X-ray diffraction patterns of a) BaC_6, b) α-phase and c) β-phase

(●) Ba (ICDD : 04-001-6704)

(●) LiCl or KCl ($ICDD_{LiCl}$: 04-016-2980 – $ICDD_{KCl}$: 04-007-3113)

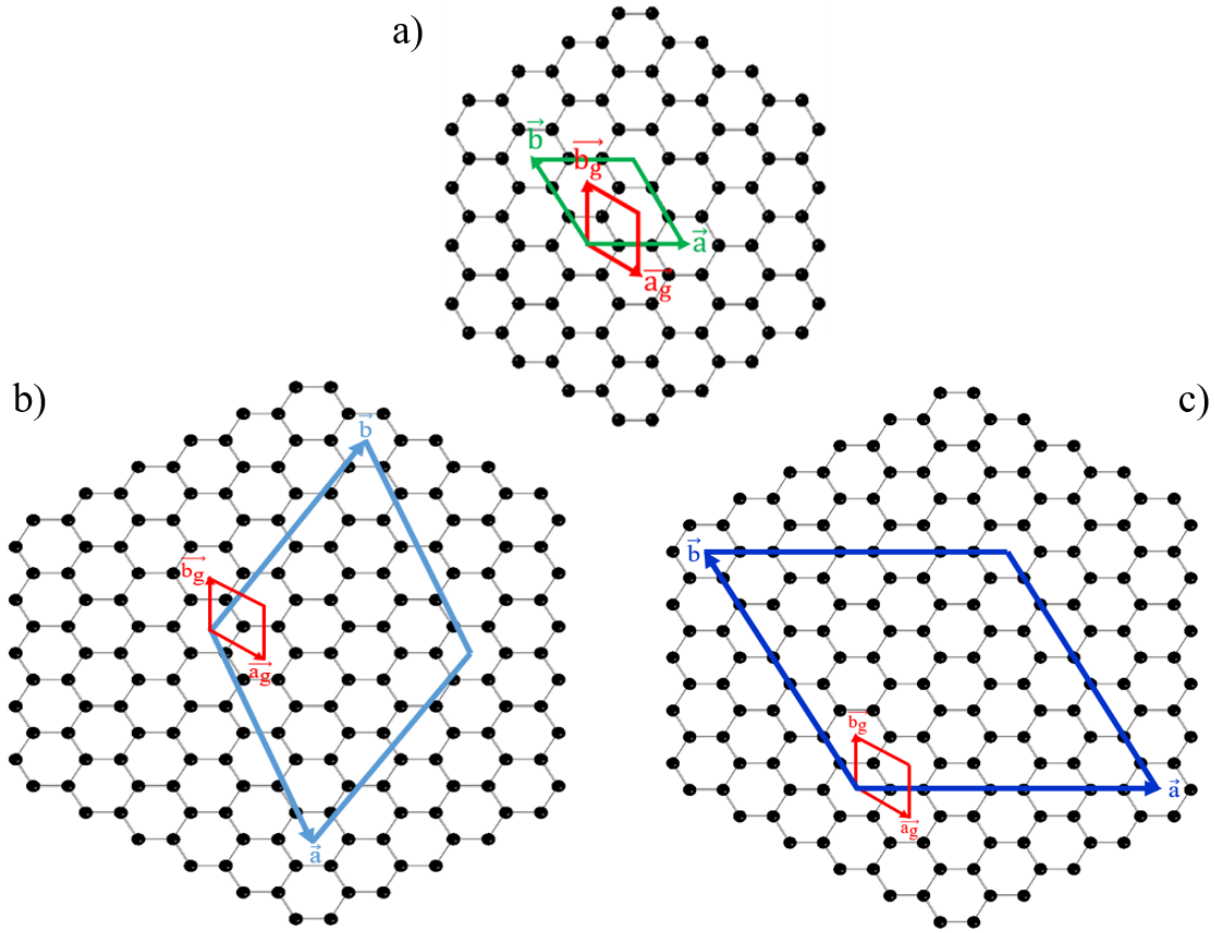

Fig. 6. 2D unit cells for a) BaC_6, b) α-phase and c) β-phase

The structural study is completed for the three compounds by rotating crystal patterns (Fig. 7) allowing to obtain the *hkl* reflections and thus to determine the c parameter. For all compounds, the 00*l* and *hk*0 reticular distances obtained thanks to these patterns are in agreement with those determined from the corresponding diffractograms.

In the case of BaC_6 (Fig. 7 a), the *hk*0 stratum confirms the value of the a parameter previously determined, and then the aforementioned $a_g\sqrt{3}$ 2D unit cell. The presence of 00*l* reflections with an even *l* number and the absence of 00*l* reflections for an odd *l* number indicate the following diffraction conditions: $l = 2n$ ($n \neq 0$), which correspond to $c = 2\ I_c = 1058.2$ pm and to a AαAβAα... (A = graphene layer; α and β = barium layers) c-axis stacking [13].

The equatorial stratum of the rotating crystal pattern relative to the α-phase (Fig. 7b) reveals that the 300 reflection is the most intense, as observed in the corresponding *kh*0 diffractogram. The indexation of the *hk*0 reflections confirms the previously mentioned 2D commensurate hexagonal unit cell with a parameter a of 1074 pm ($a = a_g\sqrt{19}$). The reflections 002 and 004 are clearly the most intense among the 00*l* ones, in agreement with the corresponding 00*l* pattern. Furthermore, the position of the *hk*1 stratum corresponds to that of the 001 reflection allowing to affirm that the c parameter corresponds to the repeat distance, *i.e.* $c = I_c = 650$ pm. The c-stacking sequence is then AαAα... (A = graphene layer; α = intercalated layer).

For the β-phase, the *kh*0 reflections observed in the equatorial stratum of the rotating crystal pattern shown figure 7c correspond to those present in the *hk*0 X-ray diagram with similar relative intensities. All these reflections can be indexed in the 2D hexagonal unit cell previously described, with $a = 3\,a_g\sqrt{3} = 1280$ pm. The 00*l* reflections are all observable up to 007, including 001, which is not visible on the 00*l* diagram. Moreover, the 003 and 006 reflections are the most intense 00*l* reflections, as observed in the 00*l* diffractogram (Fig. 3c). The simultaneous presence of the 001 and 211 reflections on the hk1 stratum allows concluding that the c parameter is equal to the repeat distance I_c, that is 950 pm. Consequently, the c-stacking sequence is AαAα... (A = graphene layer; α = intercalated layer).

This crystallographic study shows good agreement between the data recorded using several experimental X-ray diffraction methods. Each Ba-based compound exhibits a singular repeat distance, higher for the quaternary compounds than for the binary one, with a c-axis stacking leading to $c = 2I_c$ for BaC_6 and c = Ic for the two quaternaries. All 2D unit cells are hexagonal, commensurate with the graphitic one, but differ in their a parameter and their orientation with respect to that of the graphene layers.

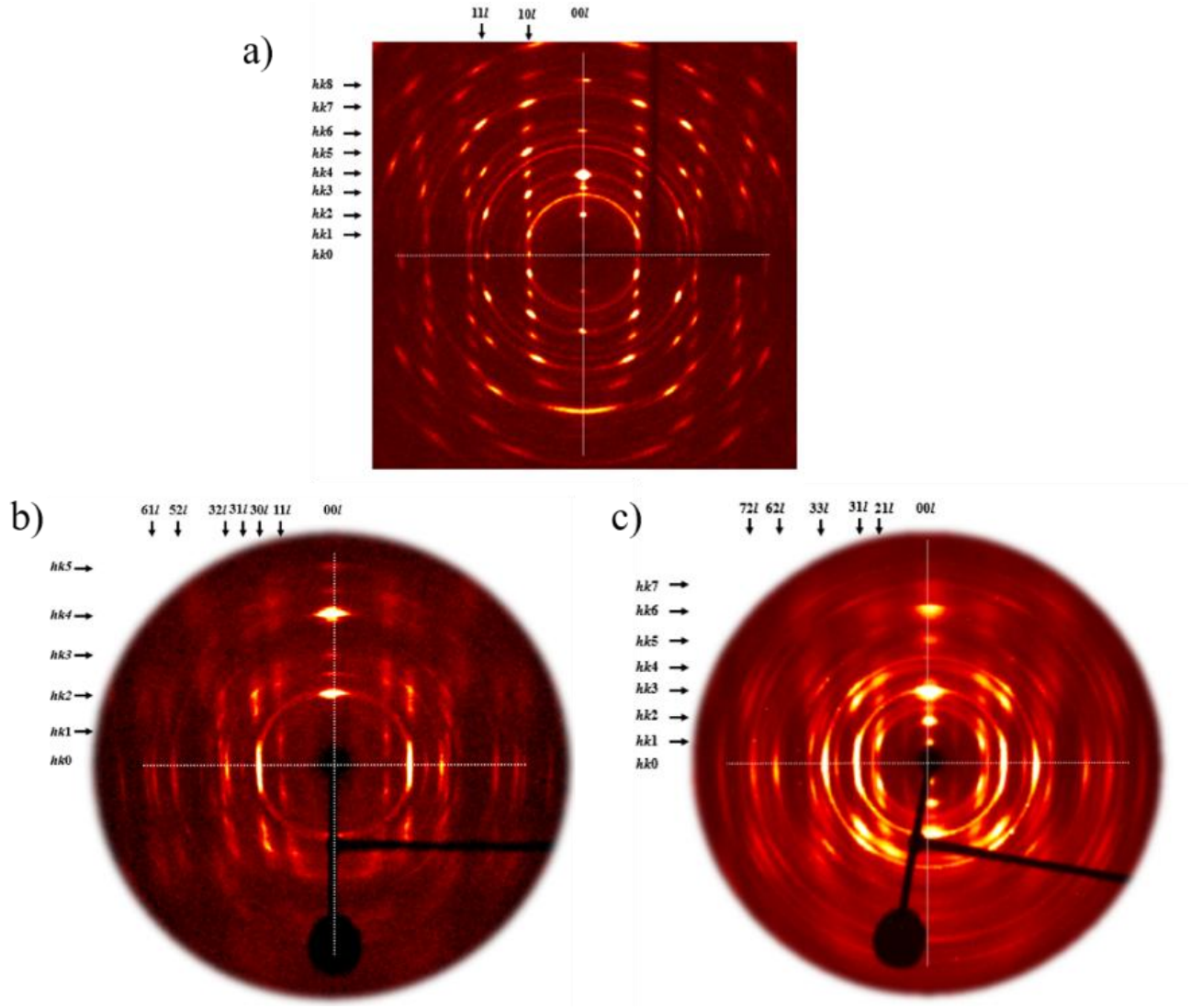

Fig. 7. Rotating crystal patterns of a) BaC_6, b) α-phase and c) β-phase

3. Reaction mechanisms

The reaction mechanisms regarding the formation of the three GIC previously described have been thoroughly examined starting from the following conditions: 2 at.% of barium dissolved in the liquid LiCl-KCl eutectic, heated at 450°C constitutes the reaction medium, in which is immersed the pyrolytic graphite platelet. The solid-liquid reaction is carried out conferring to the above detailed process. It is regularly stopped for increasing durations, in order to observe the composition of the sample over time, by means of *ex situ* X-ray diffraction. The corresponding 00*l* X-ray diffraction patterns are brought together Fig. 8. First, we can clearly

observe the color of the samples evolving over time. It is the first index, which characterizes the different steps of the reaction.

- first step: lithium intercalates alone into graphite leading to the first stage LiC_6 GIC (golden silver).

- second step: after two days, lithium is progressively expelled by barium, which intercalates in its place forming the first stage BaC_6 GIC (silver).

- third step: between the fourth and the tenth days, BaC_6 is slowly replaced by the β quaternary GIC ($Li_{0.2}K_{0.75}Ba_{0.6}C_6$) (indigo blue).

- fourth step: after eleven days, the β-phase is gradually replaced by the α one ($Li_{0.2}K_{0.6}Ba_{0.35}C_6$); the coexistence of both quaternaries side by side in the sample is manifested in the dark blue color.

- fifth step: after twelve days, the α quaternary phase remains all alone sustainably; the sample is light blue and no longer evolves over time. This α–compound constitutes the thermodynamically stable phase in the reaction conditions described above.

This whole complex mechanism is illustrated in Fig. 9. It exhibits the successive formation of the four GIC, which form during this intercalation reaction.

According to an already described substitution process, the BaC_6 binary phase is obtained from LiC_6 one. Then due to the low dissolution of the Ba^{2+} cations, the chemical activities of the K^+ and Li^+ ones are noticeably increased, so that their co-intercalation occurs after four days of reaction. Simultaneously an incomplete de-intercalation of barium happens, inducing a splitting of the metallic central layer into two sheets. Overall the amount of intercalated metals is strongly increased (55% for the transition from BaC_6 to the β-phase), which explains the large growth of the spacing of the graphene planes (80%).

Thereafter a part of intercalated potassium and barium are evacuated from graphite simultaneously with a coalescence of both barium layers into a central single one. These phenomena are accompanied by a remodeling of the remaining potassium and lithium into two symmetrical layers on either side of the central barium plane. In the end, the shrinkage of the interplanar distance (31.5% during the transition from β to α) occurs, with a decrease of the amount of intercalated metals of 25.8%.

Using absolutely constant reaction conditions, it is interesting to observe that the three Ba-based GIC appear successively over time. Only the last one (α-phase) is stable in these conditions, since even after three weeks this unique compound remains within the reaction liquid. The synthesis of this latter compound is peculiarly complex. Indeed, three different GIC have to be formed beforehand and successively in order to obtain this quaternary phase.

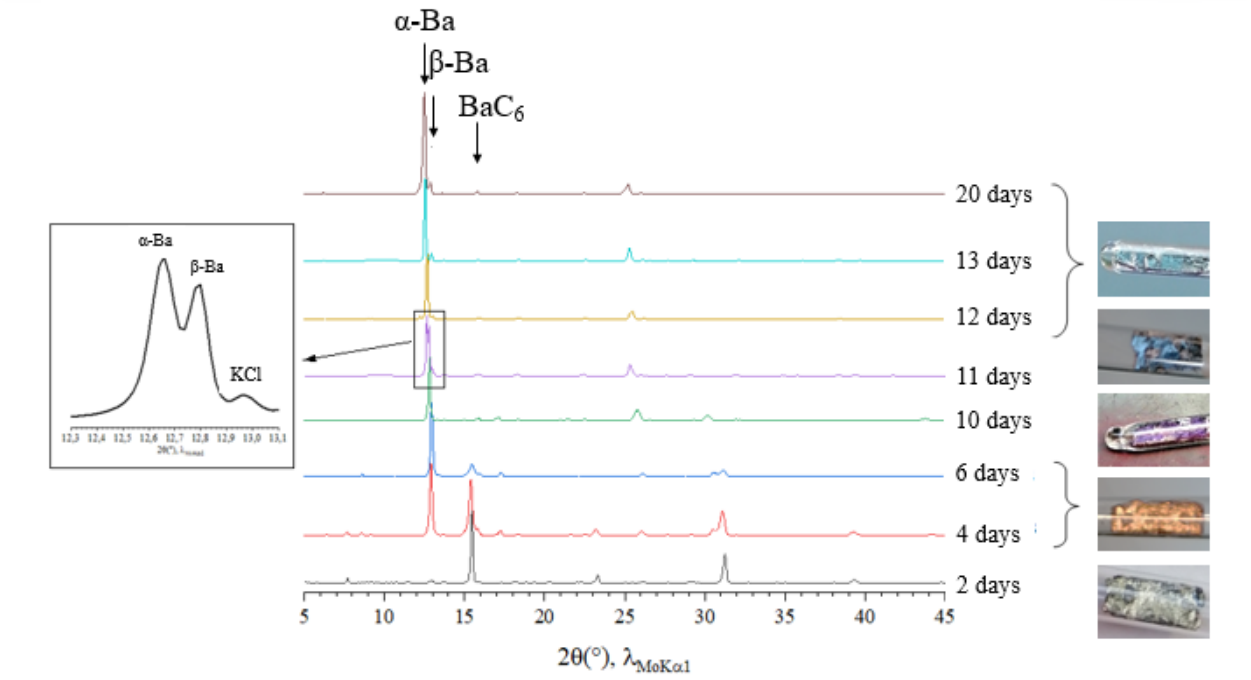

Fig. 8. *Ex situ* 00*l* X-ray diffraction patterns and pictures of the related samples, for several reaction times (2 at.% of barium in LiCl-KCl eutectic at 450°C).

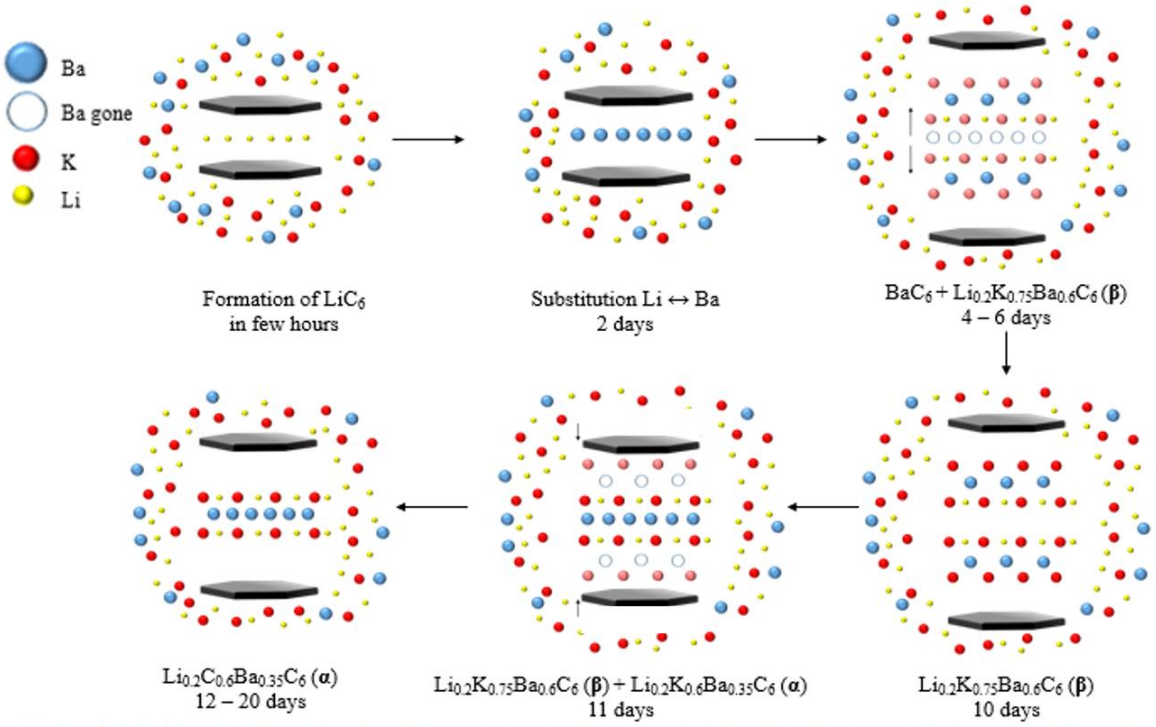

Fig. 9. Intercalation mechanism leading to the α-phase.

Conclusion

Solid-gas or solid-liquid reaction in alkali-based molten alloys exhibit limitations for intercalation reactions into graphite. That is why we investigated the reactivity of graphite versus different metal/LiCl-KCl systems. In this paper, we explore barium reactivity towards graphite in the LiCl-KCl eutectic molten salt. Using 2at.% of Ba in the eutectic mixture at 450°C, four first-stage compounds have been evidenced and a formation mechanism is suggested thanks to *ex situ* XRD analysis. First, barium is oxidized by Li^+ ions and native Li^0 achieves the formation of LiC_6. Then, due to this pre-opening of van der Waals galleries of graphite, a substitution between lithium and barium occurs, hence giving the first stage BaC_6 GIC. In fact, this well-known binary compound does not appear to be the thermodynamically stable compound. Indeed, for longer reaction times, atomic rearrangements lead to the formation of a β-phase, and finally the α-phase is formed. For the β-compound, the amount of intercalated metals is the highest with a $Li_{0.2}K_{0.75}Ba_{0.6}C_6$ chemical formula. A complex K-Ba-(K/Li)-(Li/K)-Ba-K stacking sequence is built by the intercalated sheet, with a 950 pm repeat distance value. This β-phase is also a reaction intermediate as the finally stable GIC is the α-phase. Its repeat distance is equal to 650

pm, and this decreasing is in agreement with the evidenced c-axis stacking sequence (Li/K)-Ba-(Li/K) for a $Li_{0.2}K_{0.6}Ba_{0.35}C_6$ chemical formula where metallic atoms have been evacuated from van der Waals galleries. For the three Ba-based compounds, 2D unit cells have been determined and are commensurate with the 2D unit cell of graphite, even in the case of very thick poly-layered intercalated sheets. Regarding the fact that we are now able to isolate each Ba-based GIC, complementary studies by X-ray diffraction or Raman spectroscopy can be envisaged especially in order to evaluate the influence of the alkali metal layers on the charge transfer as the latter can be directly correlated with the physical properties.

Funding source

The authors claim that no funding source is involved in this research article.

References

[1] V. K. Fredenhagen, G. Cadenbach. Die bindung von kalium durch kohlenstoff. Z. Anorg. Allg. Chem. 158, 249-263 (1926).

[2] A. Hérold. Recherches sur les composes d'insertion du graphite. Bull. Soc. Chim. Fr. 999 (1955).

[3] D. Guérard, A. Hérold. Intercalation of lithium into graphite and other carbons. Carbon 13, 337-345 (1975).

[4] J. Asenbauer, T. Eisenmann, M. Kuenzel, A. Kazzazi, Z. Chen, D. Bresser. The success story of graphite as a lithium-ion anode material – fundamentals, remaining challenges, and recent developments including silicon (oxide) composites. Sustainable Energy Fuels, 4, 5387-5416 (2020).

[5] N. Emery, C. Hérold, P. Lagrange. The synthesis of binary metal-graphite intercalation compounds using molten lithium alloys. Carbon 46, 72-75 (2008).

[6] I. El Hajj, L. Speyer, S. Cahen, P. Lagrange, G. Medjahdi, C. Hérold. Crystal structure of first stage strontium-graphite intercalation compound. Carbon 168, 732-736 (2020).

[7] N. Emery, C. Hérold, M. d'Astuto, V. Garcia, C. Bellin, J.F. Marêché, P. Lagrange, G. Loupias. Superconductivity of bulk CaC_6. Phys. Rev. Lett. 95 (2005) 87003.

[8] J. S. Kim, L. Boeri, J. R. O'Brien, F. S. Razavi & R. K. Kremer. Superconductivity in heavy alkaline-earth intercalated graphite. Phys. Rev. Lett. 99, 027001 (2007).

[9] S. Heguri, N. Kawade, T. Fujisawa, A. Yamaguchi, A. Sumiyama, K. Tanigaki & M. Kobayashi. Superconductivity in the graphite intercalation compound BaC_6. Phys. Rev. Lett. 114, 247201 (2015).

[10] D. Guérard, M. Chaabouni, P. Lagrange, M. El Makrini, A. Hérold. Insertion de métaux alcalino-terreux dans le graphite. Carbon 18, 257-264 (1980).

[11] S. Pruvost, C. Hérold, A. Hérold, P. Lagrange. Structural study of novel graphite-lithium-calcium intercalation compounds, Eur. J. Inorg. Chem. 2004, 1661-1667 (2004).

[12] M. Fauchard, S. Cahen, M. Bolmont, G. Medjahdi, P. Lagrange, C. Hérold . An efficient medium to intercalate metals into graphite: LiCl-KCl molten salts. Carbon 144, 171-176 (2019).

[13] I. El Hajj, L. Speyer, S. Cahen**,** L. Herbuvaux, P. Lagrange, G. Medjahdi, C. Hérold. Intercalation of barium into graphite by molten salts method: Synthesis of massive samples for crystal structure determination of BaC_6. Carbon 186, 431-436 (2022).

[14] I. El Hajj, L. Speyer, S. Cahen, P. Berger, G. Medjahdi, P. Lagrange, C. Hérold. Simultaneous intercalation of lithium, potassium and strontium into graphite in molten salts medium. J. Sol. State Chem. 320, 123824 (2023).

[15] I. El Hajj, L. Speyer, S. Cahen, P. Berger, G. Medjahdi, P. Lagrange, C. Hérold. Co-intercalation into graphite of lithium, potassium and barium using LiCl–KCl molten salt. Carbon Lett. (2022).

[16] A. S. Basin, A. B. Kaplun, A. B. Meshalkin, N. F. Uvarov. The LiCl-KCl binary system. Russ. J. Inorg. Chem. 53, 1509–1511 (2008).

[17] S. Y. Leung, M. S. Dresselhaus. Structural studies of graphite intercalation compounds using (00*l*) X-ray diffraction. Phys. Rev. B Condens. Matter Mater. Phys. 24, 3505-3518 (1981).

[18] R. Amirikas, D. N. Jamieson, S. P. Dooley, Measurement of (p, p) elastic cross sections for C, O and Si in the energy range 1.0-3.5 MeV, Nucl. Instrum. Methods in Physics Res. B. 77, 110-116 (1993). https://doi.org/10.1016/0168-583X(93)95531-9

[19] A. F. Gurbich, Evaluation of non-Rutherford proton elastic scattering cross section for oxygen, Nucl. Instrum. Methods in Physics Res. B. 129, 311-316 (1997). https://doi.org/10.1016/S0168-583X(97)00288-7

[20] I. Bogdanović, S. Fazinić, M. Jakšić, T. Tadić, O. Valković, V. Valković, Proton elastic scattering from fluorine, chlorine, zinc, selenium and bromine in the energy region from 2.5 to 4.8 MeV, Nucl. Instrum. Methods in Physics Res. B. 79, 524-526 (1993). https://doi.org/10.1016/0168-583X(93)95405-T

[21] R. J. De Meijer, A. A. Sieders, H. A. A. Landman, G. De Roos, Investigation of proton induced resonance reactions on 39 K, Nucl. Phys. A. 155, 109-128 (1970). https://doi.org/10.1016/0375-9474(70)90081-3

[22] S. Bashkin, H. T. Richards, Proton bombardment of the lithium isotopes, Phys. Rev. 84, 1124-1129 (1951). https://doi.org/10.1103/PhysRev.84.1124

[23] M. Mayer. Proceedings, 15th International Conference on the Application of Accelerators in Research and Industry 475, 541-544 (1999). https://doi.org/ 10.1063/1.59188

[24] P. Lagrange, M. Fauchard, S. Cahen, C. Hérold. Exhaustive inventory of 2D unit cells commensurate with honeycomb graphene structure. Carbon 94, 919-927 (2015). https://doi.org/10.1016/j.carbon.2015.07.060